SUPPORTING INFORMATION

Achieving 9% EQE in Light-Emitting Electrochemical Cells via TADF-Sensitized Fluorescent Strategy

Zeyang Zhou[†], Qingda Chang[†], Rui Chen, Pengfei Jin, Baipeng Yin,* Chuang Zhang,* and Jiannian Yao


Z. Zhou, Q. Chang, Dr. R. Chen, P. Jin, Dr. B. Yin, Prof. C. Zhang, Prof. J. Yao
Key Laboratory of Photochemistry
Beijing National Laboratory for Molecular Sciences
Institute of Chemistry, Chinese Academy of Sciences
Beijing 100190, China
E-mail: yinbaipeng@iccas.ac.cn; zhangc@iccas.ac.cn

Z. Zhou, Q. Chang, Dr. R. Chen, P. Jin
University of Chinese Academy of Sciences
Beijing 100049, China

Prof. J. Yao
Institute of Molecular Engineering Plus
Fuzhou University
Fuzhou 350108, China

[†]These   authors   have   made   equal   contributions   to   this   work.
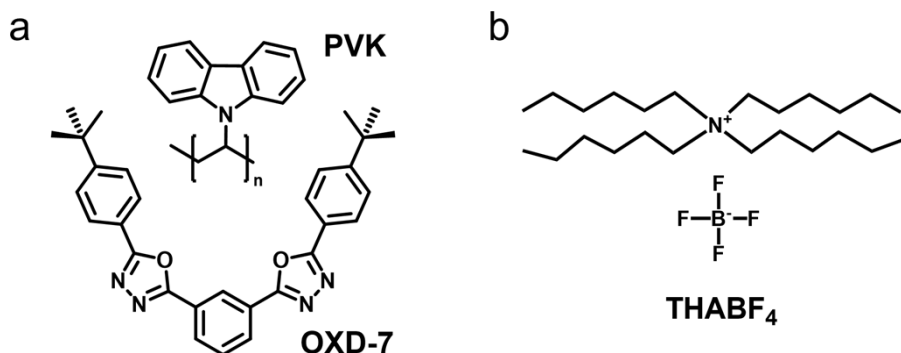
**Figure S1.** Molecule structure of mixed host includes PVK and OXD-7, and the electrolyte THABF$_4$.
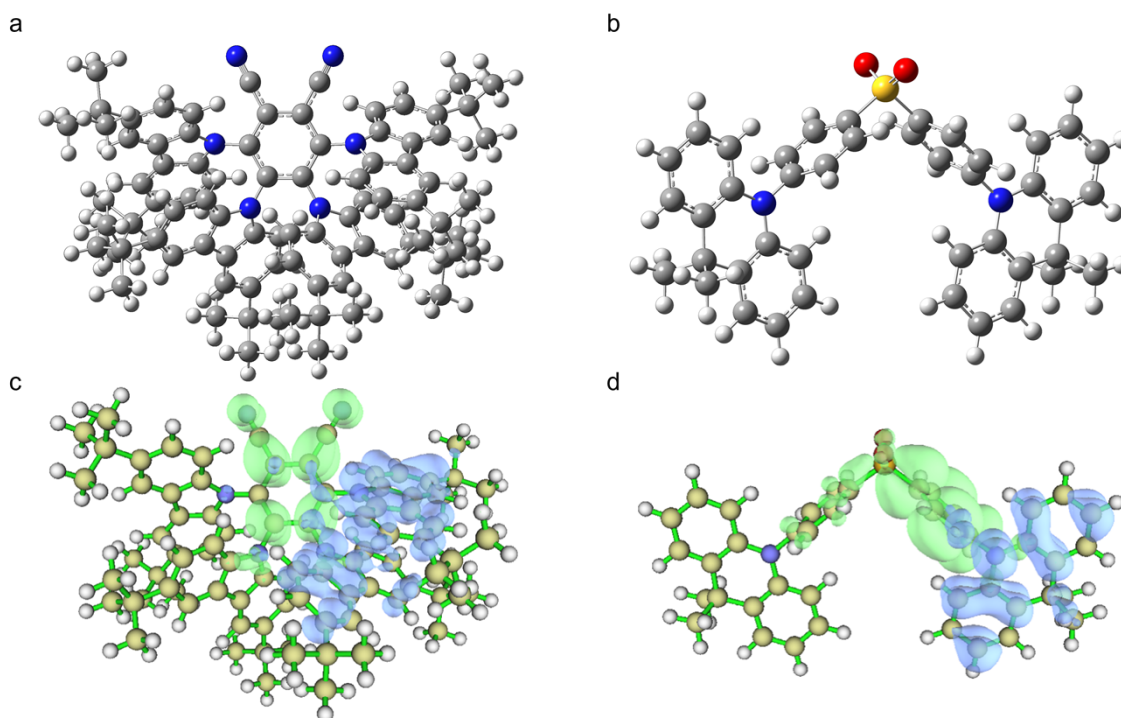
Figure S2. (a) Ground state (S$_0$) geometry of 4CzPN-tBu. (b) Ground state (S$_0$) geometry of DMAC-DPS. (c) Electron-hole analysis of 4CzPN-tBu. (d) Electron-hole analysis of DMAC-DPS. The blue represents the holes and the green represents the electrons.

we performed theoretical calculations on the sensitizer DMAC-DPS and the emitter 4CzPN-tBu. As shown in Figure S2a,b, the ground state (S$_0$) geometries of both molecules were optimized in the gas phase using Density Functional Theory (DFT) with the M062X functional and the 6-31G(d) basis set. Subsequently, geometry optimizations for the first excited singlet (S$_1$) and triplet (T$_1$) states were performed using time-dependent DFT (TD-DFT) with the same functional and basis set, and the electron-hole analysis based on the results are depicted in Figure S2c,d to display the molecule's charge transfer excitation characteristics[1–3]. The M06-2X functional is a hybrid meta-generalized gradient-approximation functional, yields an intermediate value for ΔE_{ST} without

overestimating or underestimating it[4]. Using M06-2X/6-31G(d), the calculated ΔE_{ST} values for DMAC-DPS and 4CzPN-tBu are 274 meV and 360 meV, respectively, which is consistent with the experimental observation that DMAC-DPS possess a more rapid RISC rate. Moreover, by considering solvent effects using the polarizable continuum model, the calculated emission wavelength for DMAC-DPS and 4CzPN-tBu are 402.82 nm and 452.21 nm, respectively, which are reasonably close to the experimentally obtained photoluminescence peak at ~460 nm and ~530 nm.
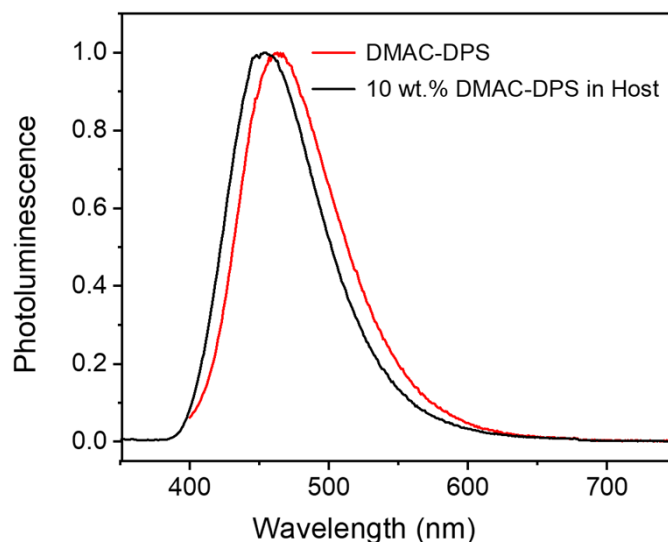

Figure S3. PL spectra measured from pristine DMAC-DPS and 10 wt.% DAMC-DPS doped in host PVK:OXD-7.

The emission spectrum of the DMAC-DPS/PVK:OXD-7 doped films is consistent with that of the pristine DMAC-DPS film. There is no host emission in the spectrum of doped sample, and small differences between doped and pristine samples may be due to instrumental error.
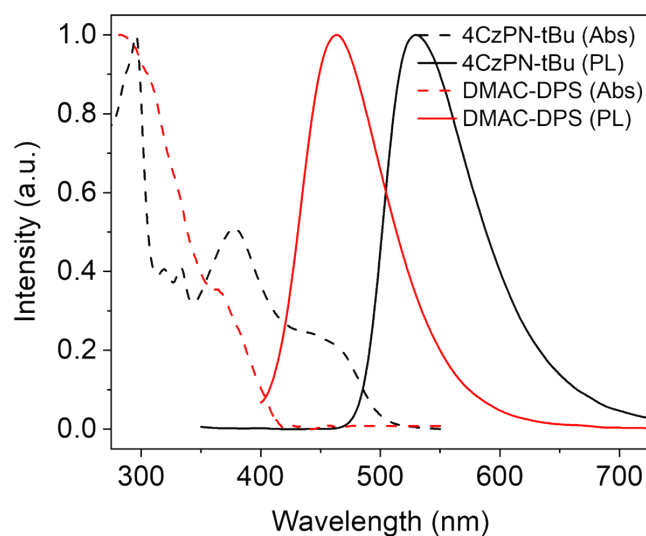
Figure S4. Absorption spectra (red solid line) and emission spectra (red dashed line) of DMAC-DPS; absorption spectra (black solid line) and emission spectra (black dashed line) of 4CzPN-tBu.
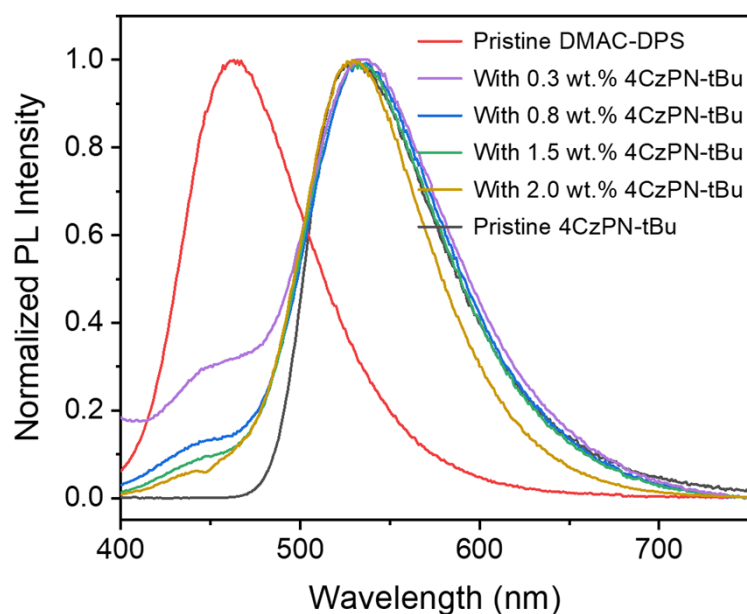
Figure S5. PL spectra obtained from the films composed of a host (PVK:OXD-7), 10 wt.% sensitizer, doped with various concentrations of 4CzPN-tBu (0 wt.%, 0.3 wt.%, 0.8 wt.%, 1.5 wt.% and 2.0 wt.%).
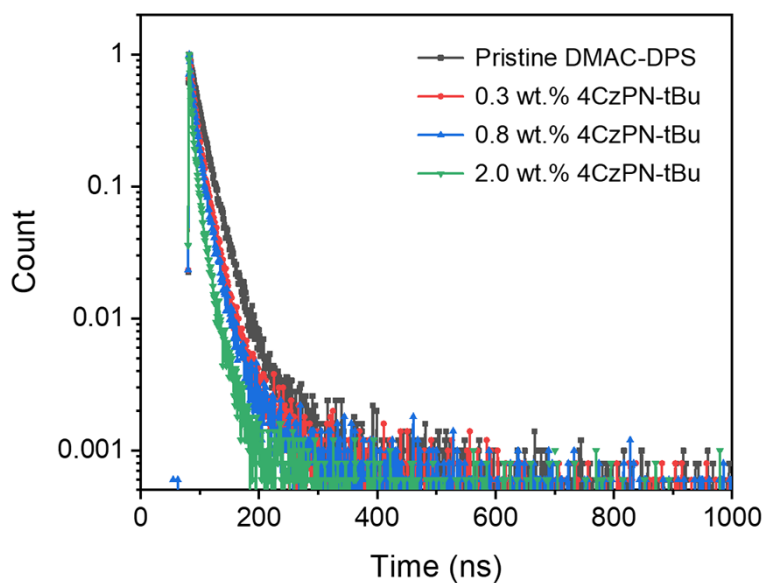
Figure S6. The fluorescence lifetime curves of the sensitizer emission at 463 nm were measured under different doping concentrations (0 wt.%, 0.3 wt.%, 0.8 wt.%, 2.0 wt.%) of the sensitizer.

463 nm is the position of the emission peak of the sensitizer and the decreased lifetime with the increasing emitter concentration represents a gradually enhanced energy transfer from sensitizer to emitter.
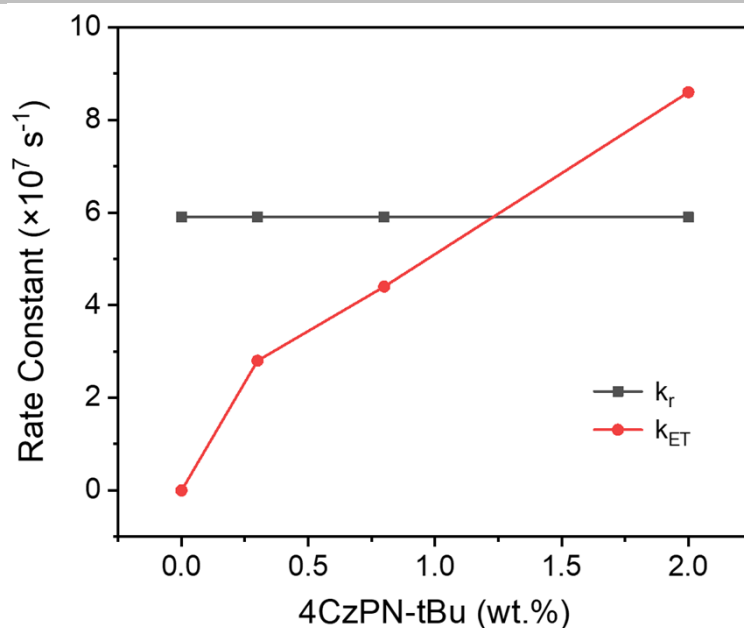
Figure S7. The radiative rate (k_r) of DMAC-DPS and the energy transfer rate (k_{ET}) from DMAC-DPS to 4CzPN-tBu as a function of 4CzPN-tBu concentration.

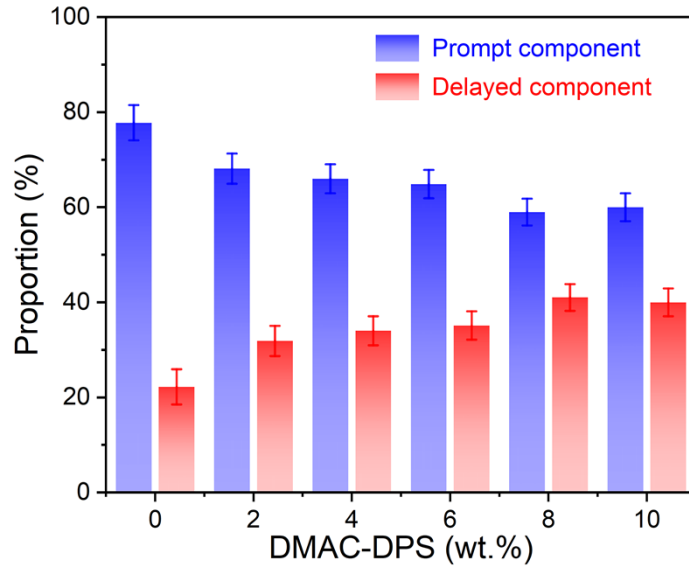$$k_{ET} = \frac{1}{\tau_p} - k_r$$

(S1)

The energy transfer rate (k_{ET}) can be calculated by **Equation S1**.
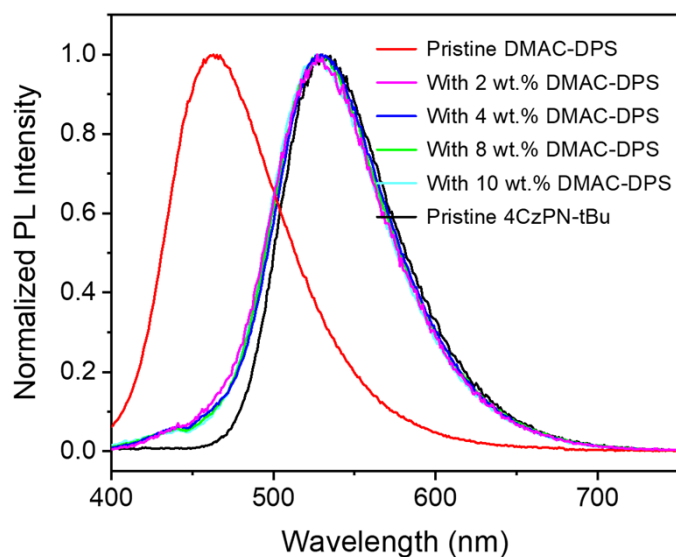
Figure S8. The PL spectra of films doped with sensitizers (0 wt.%, 2.0 wt.%, 4.0 wt.%, 8.0 wt.%, 10.0 wt.%) in the host of PVK:OXD-7.

Figure S9. The proportion of the two components obtained by decomposition varies with the concentration of DMAC-DPS.

The life decay curve in Figure 3 can be fitted with the equation S2 to obtain the lifetime of the two components. And their proportion can be calculated by equation S3 and equation S4 and has been plotted in Figure S8. By multiplying the photoluminescence quantum yield by the proportion of the two components respectively，we can obtain their contribution to the total photoluminescence quantum yield.

$$A = A_0 + A_1 \exp\left(-t/\tau_p\right) + A_2 \exp\left(-t/\tau_d\right) \tag{S2}$$

$$Proportion_p = \frac{A_1 \tau_p}{A_1 \tau_p + A_2 \tau_d} \tag{S3}$$

$$Proportion_d = \frac{A_2 \tau_d}{A_1 \tau_p + A_2 \tau_d} \tag{S4}$$
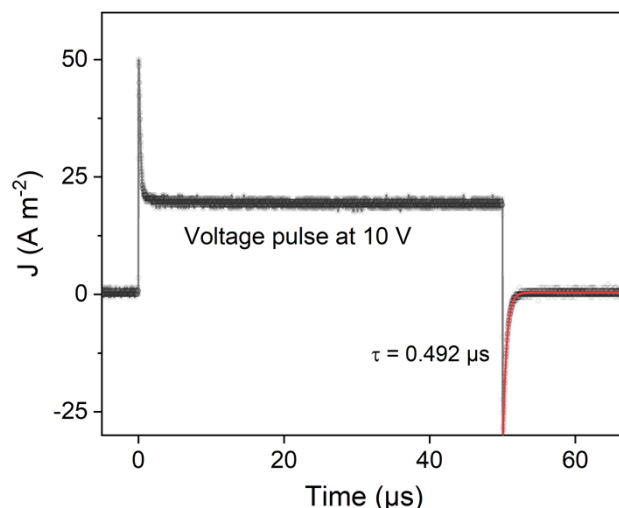
Figure S10. The current response of LECs without sensitizer under a pulse at 10 V and the exponentially fitted curve of the second current spike.

A typical transient current characteristic of LECs driven with voltage pulses is shown in Figure S10. A current spike occurs almost immediately after pulse onset, followed by the current relaxation to a certain steady-state value. At the end of the voltage pulse, negative current spike occurs before relaxing to zero amps. As previously reported in the literature [5], the RC time constant can be obtained by fitting the transient current response at the negative current spike through Equation S5. Therefore, the RC time constant was determined to be 0.492 μs, which is significantly shorter than the EL decay time, indicating that the RC effect has a negligible impact on transient EL.

$$J(t) = J_{spike}\exp\left(-\frac{t - t_{spike}}{\tau_{RC}}\right)$$

(S5)

Where $J(t)$ is the current density of time t, J_{spike} is the current density when the negative spike starts, tspike is the time when the negative spike starts and τ_{RC} is the RC time constant.

Reference

1   T. Lu, A comprehensive electron wavefunction analysis toolbox for chemists, Multiwfn, *J. Chem. Phys.*, 2024, **161**, 082503.

2   Z. Liu, T. Lu and Q. Chen, An sp-hybridized all-carboatomic ring, cyclo[18]carbon: Electronic structure, electronic spectrum, and optical nonlinearity, *Carbon*, 2020, **165**, 461–467.

3   T. Lu and F. Chen, Multiwfn: A multifunctional wavefunction analyzer, *J. Comput. Chem.*, 2012, **33**, 580–592.

4   H. Uoyama, K. Goushi, K. Shizu, H. Nomura and C. Adachi, Highly efficient organic light-emitting diodes from delayed fluorescence, *Nature*, 2012, **492**, 234–238.

5   V. Ahmad, J. Sobus, M. Greenberg, A. Shukla, B. Philippa, A. Pivrikas, G. Vamvounis, R. White, S.-C. Lo and E. B. Namdas, Charge and exciton dynamics of OLEDs under high voltage nanosecond pulse: towards injection lasing, *Nat. Commun.*, 2020, **11**, 4310.